Materials Letters 65 (2011) 3540–3543

Contents lists available at ScienceDirect

Materials Letters

journal homepage: www.elsevier.com/locate/matlet

Anomalous activation of shallow B^+ implants in Ge

B.R. Yates [a,*], B.L. Darby [a], N.G. Rudawski [a], K.S. Jones [a], D.H. Petersen [b], O. Hansen [b,c], R. Lin [d], P.F. Nielsen [d], A. Kontos [e]

[a] Department of Materials Science and Engineering, University of Florida, Gainesville, FL 32611-6400, United States
[b] Department of Micro- and Nanotechnology, Technical University of Denmark, DTU Nanotech, Building 345B, DK-2800 Kgs. Lyngby, Denmark
[c] Center for Individual Nanoparticle Functionality, CINF, Technical University of Denmark, DK-2800 Kgs. Lyngby, Denmark
[d] CAPRES A/S, Scion-DTU, DK-2800 Kgs. Lyngby, Denmark
[e] Varian Semiconductor Equipment Associates, Gloucester, MA 01930, United States

ARTICLE INFO

Article history:
Received 3 May 2011
Accepted 28 July 2011
Available online xxxx

Keywords:
Ge
B
Dopant activation
Micro four point probe
TEM

ABSTRACT

The electrical activation of B^+ implantation at 2 keV to doses of 5.0×10^{13}–5.0×10^{15} cm^{-2} in crystalline and pre-amorphized Ge following annealing at 400 °C for 1.0 h was studied using micro Hall effect measurements. Preamorphization improved activation for all samples with the samples implanted to a dose of 5.0×10^{15} cm^{-2} displaying an estimated maximum active B concentration of 4.0×10^{20} cm^{-3} as compared to 2.0×10^{20} cm^{-3} for the crystalline sample. However, incomplete activation was observed for all samples across the investigated dose range. For the sample implanted to a dose of 5.0×10^{13} cm^{-2}, activation values were 7% and 30%, for c-Ge and PA-Ge, respectively. The results suggest the presence of an anomalous clustering phenomenon of shallow B^+ implants in Ge.

1. Introduction

As the scaling associated with traditional Si metal oxide semiconductor (MOS) devices reaches fundamental limits, changes in MOS design or material composition are becoming necessary. Ge is a promising alternative material for next-generation MOS devices as its increased carrier mobility makes it an attractive replacement for Si [1]. In addition, its reduced melting temperature may allow for less aggressive annealing recipes which could prove advantageous for process integration of high-κ/metal gate device structures.

In the case of B, it is known that the equilibrium chemical solid solubility limit in Ge [2] is 5.5×10^{18} cm^{-3} at 850 °C, which is significantly lower compared to Si at the homologous temperature [3,4]. However, electrical activation in excess of this value was reported for B^+-implantation into single-crystal (c) as well as pre-amorphized (PA) material [5–11]. For B^+ implants at 35 keV into PA-Ge, complete activation was observed for all doses up to 7.6×10^{15} cm^{-2} implying active B concentrations as high as 5.7×10^{20} cm^{-3} following an anneal at 360 °C for 1.0 h [10]. In the case of PA-Ge, annealing to induce solid-phase epitaxial growth (SPEG) of the amorphized layer results in the incorporation of a concentration of substitutional B greater than the equilibrium chemical concentration; analogous behavior was similarly reported for the case of B^+-implantation into Si [12].

Although B activation has been characterized for deep B^+-implantation into both c-Ge and PA-Ge, the activation of low energy B^+-implantation in Ge remains poorly understood and characterized. In the few studies which utilized low energy B^+-implantation, the activation level, if determined, was calculated indirectly by fitting resistance values to a mobility model [7,9,13]. This model was developed using Hall effect measurements and may suffer from possible error introduced from Hall scattering factor assumptions [14]. In order to accurately characterize the activation behavior, the sheet carrier density and mobility should be measured directly using a Hall effect technique.

Furthermore, characterization of shallow implant activation is very challenging with conventional four-point probe and Hall effect techniques partially due to high junction leakage [15–17]. Due to the smaller band gap of Ge compared to Si and the larger number of intrinsic carriers [1], junction leakage is increased for Ge [18,19] which exacerbates the characterization challenges. Recently, instruments and techniques have been developed which perform four-point probe and Hall effect measurements using probes with μm-scale spacing as described in detail elsewhere [17,20–22]; these micro four-point probe (M4PP) and micro Hall effect (MHE) measurements have been shown to greatly reduce the effects of junction leakage [15–17] and have previously been used for successful characterization of active shallow dopants in Ge [8,23]. In this work, the activation of low energy B^+-implantation into c-Ge and PA-Ge was studied using M4PP and MHE measurements.

2. Experimental

Czochralski-grown n-type (001) wafers (resistivity ~ 50 Ω cm) were used for this work. A set of c-Ge samples was produced by

* Corresponding author. Tel.: +1 352 846 3353; fax: +1 352 392 7219.
E-mail address: bradyates@ufl.edu (B.R. Yates).

0167-577X/$ – see front matter © 2011 Elsevier B.V. All rights reserved.
doi:10.1016/j.matlet.2011.07.093

B^+-implantation at 2 keV to doses of 5.0×10^{13}–5.0×10^{15} cm^{-2} while a set of PA-Ge samples was produced by first performing Ge^+-implantation at 120 keV to a dose of 2×10^{14} cm^{-2} before the same B^+-implantation step. In the case of PA-Ge samples, a continuous amorphous layer extending 100 ± 2.5 nm from the surface was produced as verified by high-resolution cross-sectional transmission electron microscopy (HR-XTEM). Samples were annealed in N_2 ambient at 400 °C for 1.0 h to activate the implanted B^+. HR-XTEM was used to image the microstructure of the specimens before and after annealing with samples prepared using focused ion beam (FIB) milling. Secondary ion mass spectrometry (SIMS) was performed on selected samples to determine B concentration profiles before and after annealing.

3. Results and discussion

Sheet resistance, Hall sheet number (n_H), and Hall mobility (μ_H) were measured using a CAPRES microRSP M-150 M4PP with Au-coated probes, a probe spacing of 20 μm, and a permanent magnet with a magnetic flux density of 0.475 T. Hall sheet number and mobility values were adjusted to obtain the carrier sheet number (n_s) and drift mobility (μ_d) by using a scattering factor (r_H) of 1.21 as determined empirically by Mirabella et al. for high dose B^+-implantation into Ge [10]. The carrier density and drift mobility are related to the Hall values by $n_s = n_H \times r_H$ and $\mu_d = \mu_H / r_H$, respectively.

Fig. 1 presents measured R_s and n_s values as a function of implanted B^+ dose for both c-Ge and PA-Ge samples following annealing at 400 °C for 1.0 h. As shown in Fig. 1a, the R_s value decreases with increasing B^+ dose for both c-Ge and PA-Ge samples with c-Ge samples exhibiting higher sheet resistance values compared to the PA-Ge samples. The reduced R_s values for the PA-Ge samples are explained by the increased solubility and B incorporation during SPEG as previously reported by others for different implant conditions [5–7]. The carrier sheet number is plotted as a function of implanted B^+ dose for both c-Ge and PA-Ge samples after adjustment with a Hall scattering factor of 1.21 as shown in Fig. 1b; the PA-Ge samples exhibited higher n_s values compared to c-Ge samples, similar to previous reports [5–7]. More interestingly, for B^+ doses less than 5.0×10^{15} cm^{-2}, the percent activation for both c-Ge and PA-Ge samples is relatively independent of dose at ~7 and ~30%, respectively. At a dose of 5.0×10^{15} cm^{-2}, the difference in percent activation is much smaller, ~10 and 15% for c-Ge and PA-Ge samples, respectively. Fig. 2 shows HR-XTEM images of a c-Ge sample B^+-implanted at 2 keV to a dose of 5.0×10^{15} cm^{-2}. As shown in Fig. 2a, a damage layer extending 18 ± 0.5 nm from the surface is evident, which matches well with the expected range [24] of the implant. At higher magnifications, as shown in Fig. 2b, amorphous pockets are evident within the damaged layer. Thus, the smaller difference in R_s between c-Ge and PA-Ge for the case of a B^+ dose of 5.0×10^{15} cm^{-2} is likely due to enhanced incorporation of substitutional B within the amorphous regions during SPEG upon annealing.

To better understand the activation behavior, samples B^+-implanted to doses of 5.0×10^{13} and 5.0×10^{15} cm^{-2} into c-Ge and PA-Ge were analyzed using SIMS before and after annealing to

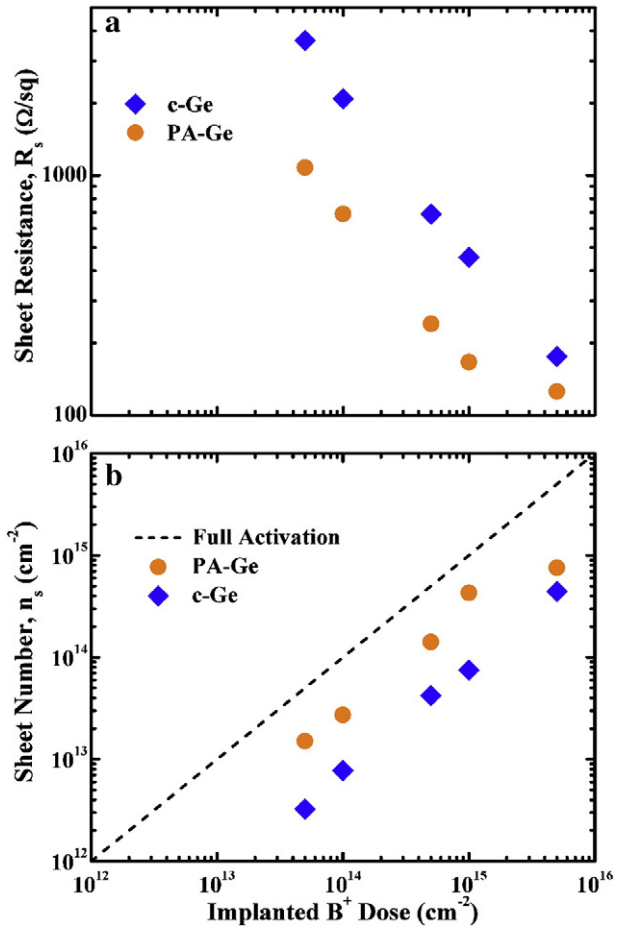

Fig. 1. (a) Measured sheet resistance (R_s) and (b) sheet number (n_s) as a function of B^+ dose implanted at 2 keV into crystalline (◆) and preamorphized (●) Ge, respectively, after annealing at 400 °C for 1 h.

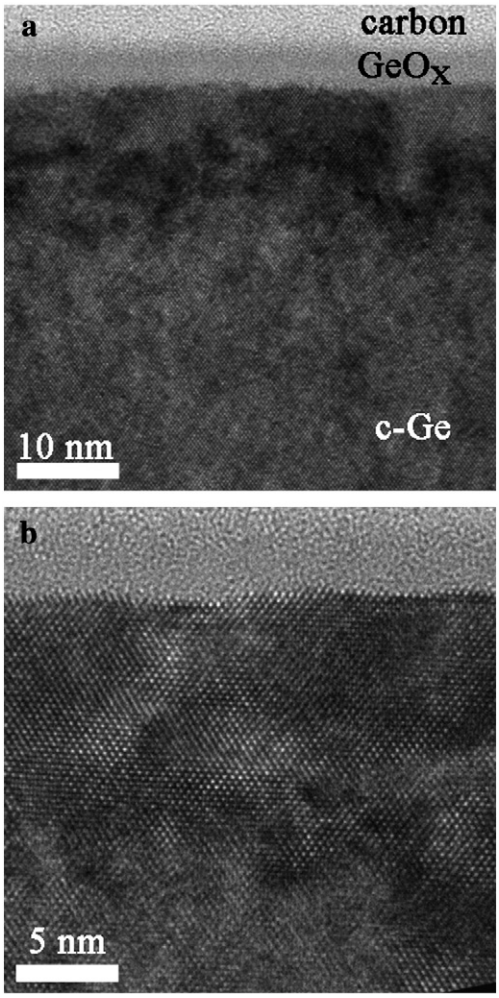

Fig. 2. HR-XTEM micrographs of an as-implanted crystalline Ge sample B^+ implanted at 2 keV to 5.0×10^{15} cm^{-2} showing: (a) a surface GeO_x layer and a damaged layer extending 18 nm from surface and (b) amorphous pockets in close proximity to the surface.

determine B concentration profiles, as shown in Fig. 3. The measured B concentration profiles (both before and after annealing) were very similar to as-implanted simulations [24]. The maximum active concentration was estimated using the SIMS profile and the corresponding measured n_s values presented in Fig. 1b as described elsewhere [6]. For c-Ge and PA-Ge samples B^+-implanted to a dose of 5.0×10^{15} cm^{-2}, the maximum active B concentrations were estimated at 2.0×10^{20} and 4.0×10^{20} cm^{-3}, respectively; the value for PA-Ge is similar to prior results [5–10].

The observed activation behavior for both c-Ge and PA-Ge samples is very interesting; incomplete activation is observed for even the lowest B^+ doses in both sample sets. Based on the reported maximum active B concentration [10], full activation should be expected for B^+-implantation at 2 keV to a dose of 5×10^{13} cm^{-2} for both c-Ge and PA-Ge, yet the measured percent activation in each case was ~7 and ~30%, respectively. This is unexpected and may have resulted from chemical dose loss or a unique dopant clustering/precipitation that scales with B^+ dose.

One contributing factor for the low levels of activation is dose loss during implantation resulting from backscattering of the light B^+ ions from the much heavier Ge atoms. In fact, for B^+-implantation at 2 keV into Ge, simulations [24] predict a backscattering loss of ~20% of the implanted dose. Additionally, due to the shallow nature of the implant, even slight surface oxidation is capable of consuming a non-negligible portion of the implanted B^+ dose. HR-XTEM analysis revealed the presence of a 3.0 ± 0.2 nm-thick surface GeO_x layer on all as-implanted samples, as shown in Fig. 2. As per simulations [24], ~8% of the implanted dose is rendered inactive via the presence of a GeO_x layer of this thickness. Finally, it should be noted that the percent of dose rendered inactive due to both oxidation and ion backscattering should be independent of implanted dose; however, the combination of losses due to backscattering and surface oxidation can only account for ~28% of dose loss. Thus, the bulk of the inactive fraction cannot be explained by these factors.

A probable source of inactive B is due to clustering, which has been observed and extensively studied in Si [25,26]. In the case of Si, for a given processing condition, full activation is expected for low B^+ doses until a certain concentration threshold is reached after which clustering occurs. However, for the presented data, incomplete activation is observed with the percent activation remaining relatively constant for investigated doses below 5.0×10^{15} cm^{-2}. Work by Impellizzeri et al. [11] and Bisognin et al. [27] revealed incomplete activation for B^+-implantation at 35 keV into c-Ge, which was attributed to the formation of a B-Ge cluster through the use of ion beam analysis and high-resolution X-ray diffraction, respectively. However, incomplete activation observed in this present work is much more pronounced and is observed in both c-Ge and PA-Ge samples. The physical explanation behind the observed anomalous activation behavior is unclear; however, the close proximity of the surface is a possible contributing factor. In comparing the results observed in this work with those by Impellizzeri et al. [10], the decrease in B^+ implant energy, or shifting the B profile closer to the surface, enhances the incomplete activation observed. Since it is known that defect production and annihilation can be influenced by surface proximity in Si [28], it is believed that the shallow nature of the implants in this work is exacerbating the incomplete activation observed through an enhanced formation of B-Ge clusters. For several decades, it has been known that the surface of Ge decomposes into a porous structure under high-dose irradiation [29]. Recently, it has been shown that self-implantation into Ge at a relatively modest dose of 2.0×10^{15} cm^{-2} and energy of 30 keV is sufficient to induce the formation of void clusters and the onset of the porous structure [30]. These results suggest that there may be a barrier to point defect recombination near the surface which may be promoting the formation of B-Ge clusters following shallow B^+ implantation in Ge. Further experiments are underway to indentify the underlying mechanism behind the observed anomalous activation behavior.

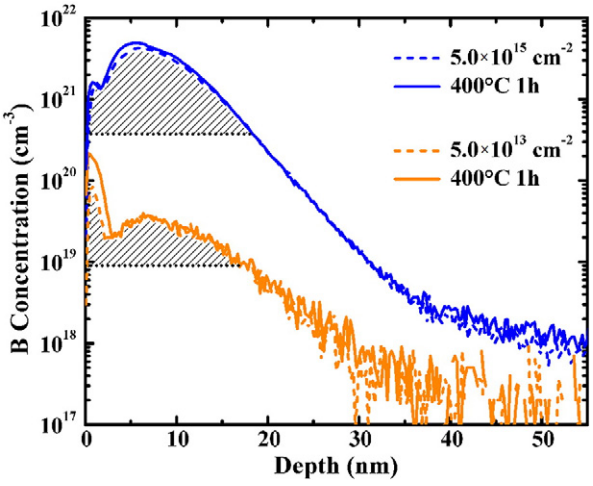

Fig. 3. B concentration profiles of a pre-amorphized Ge sample B^+-implanted at 2 keV to doses of 5.0×10^{13} (—) or 5.0×10^{15} cm^{-2} (—) as-implanted (dashed line) and after annealing at 400 °C for 1 h (solid line) as measured using SIMS. The horizontal dotted lines indicate the estimated maximum active B concentration for both implant conditions.

4. Conclusions

In summary, the activation of B^+-implantation at 2 keV into crystalline and pre-amorphized Ge was studied using micro four-point probe and micro Hall effect measurements. For B^+ doses of 5.0×10^{13}–5.0×10^{15} cm^{-2}, pre-amorphized samples exhibited greater activation compared to crystalline samples following a 400 °C anneal for 1.0 h. In the case of B^+-implantation to a dose of 5.0×10^{15} cm^{-2}, the discrepancy in activation between crystalline and pre-amorphized samples is much smaller; this was attributed to solid-phase epitaxial growth within amorphous pockets formed in crystalline samples as a result of only B^+-implantation. Interestingly, for both crystalline and pre-amorphized samples, the measured percent activation was approximately independent of implanted dose; this behavior is in stark contrast to reported activation behavior of shallow B^+-implantation in Si and deeper B^+-implantation in Ge. This indicates the possibility of a B activation mechanism which is unique to shallow B^+-implantation in Ge; the physical explanation of this anomalous behavior is unclear, though the close proximity of the surface to the implanted B^+ profile may be a contributing factor.

Acknowledgments

The authors acknowledge the Intel Corporation for funding this work and the Major Analytical Instrumentation Center at the University of Florida for use of the FIB and TEM facilities. CINF is sponsored by The Danish National Research Foundation.

References

[1] Sze SM, Ng KK. Physics of semiconductor devices. John Wiley and Sons; 2007.
[2] Uppal S, Willoughby AFW, Bonar JM, Evans AGR, Cowern NEB, Morris R, et al. J Appl Phys 2001;90:1376–80.
[3] Trumbore FA. Bell Syst Tech J 1960;39:205–33.
[4] Borisenko VE, Yudin SG. Phys Stat Sol 1987;101:123–7.
[5] Chao Y-L, Prussin S, Woo JCS, Scholz R. Appl Phys Lett 2005;87:142102.
[6] Satta A, Simoen E, Clarysse T, Janssens T, Benedetti A, De Jaeger B, et al. Appl Phys Lett 2005;87:172109.
[7] Bruno E, Impellizzeri G, Mirabella S, Piro AM, Irrera A, Grimaldi MG. Mater Sci and Eng: B 2008;56:154–5.
[8] Hellings G, Rosseel E, Clarysse T, Petersen DH, Hansen O, Nielsen PF, et al. Microelectron Eng 2011;88:347–50.
[9] Chao YL, Woo JCS. Electron devices, IEEE transactions on 2007;54:2750–5.

[10] Mirabella S, Impellizzeri G, Piro AM, Bruno E, Grimaldi MG. Appl Phys Lett 2008;92:251909.
[11] Impellizzeri G, Mirabella S, Bruno E, Piro AM, Grimaldi MG. J Appl Phys 2009;105:063533.
[12] Tsai MY, Streetman BG. J Appl Phys 1979;50:183–7.
[13] Simoen E, Brouwers G, Satta A, David M-L, Pailloux F, Parmentier B, et al. Mater Sci in Semicond Process 2008;11:368–71.
[14] Golikova OA. Sov Phys Solid State 1962;3:2259–65.
[15] Clarysse T, Moussa A, Leys F, Loo R, Vandervorst W, Benjamin MC, et al. Mater Res Soc Symp Proc 2006;912:197.
[16] Clarysse T, Bogdanowicz J, Goossens J, Moussa A, Rosseel E, Vandervorst W, et al. Mater Sci and Eng: B 2008;154–155:24–30.
[17] Petersen CL, Rong Lin, Petersen DH, Nielsen PF. IEEE international conference on advanced thermal processing of semiconductors, 153. RTP; 2006.
[18] Eneman G, Wiot M, Brugere A, Casain OSI, Sonde S, Brunco DP, et al. Electron devices IEEE transactions on 2008;55:2287–96.
[19] Claeys C, Mitard J, Eneman G, Meuris M, Simoen E. Thin Solid Films 2010;518:2301–6.
[20] Petersen DH, Hansen O, Lin R, Nielsen PF. J Appl Phys 2008;104:013710.
[21] Petersen DH, Hansen O, Lin R, Nielsen PF, Clarysse T, Goossens J, et al. IEEE international conference on advanced thermal processing of semiconductors. RTP; 2008. p. 251–6.
[22] Thorsteinsson S, Wang F, Petersen DH, Hansen TM, Kjær D, Lin R, et al. Rev Sci Instrum 2009;80:053902.
[23] Hellings G, Rosseel E, Simoen E, Radisic D, Petersen DH, Hansen O, et al. Electrochem Solid-State Lett 2011;14:H39–41.
[24] Ziegler JF. Nucl Instrum Methods Phys Res B 2004;219–220:1027–36.
[25] Cowern NEB, Janssen KTF, Jos HFF. J Appl Phys 1990;68:6191–8.
[26] Lilak AD, Law ME, Radic L, Jones KS, Clark M. Appl Phys Lett 2002;81:2244–6.
[27] Bisognin G, Vangelista. S, Berti M, Impellizeri G, Grimaldi MG. J Appl Phys 2010;107:103512.
[28] Agarwal A, Gossmann H-J, Eaglesham DJ, Pelaz L, Jacobson DC, Poate JM, et al. Mater Sci and Eng A 1998;253:269–74.
[29] Appleton BR, Holland OW, Narayan J, Schow OE, Williams JS, Short KT, et al. Appl Phys Lett 1982;41:711–2.
[30] Darby BL, Yates BR, Rudawski NG, Jones KS, Kontos A, Elliman RG. Thin Solid Films 2011;519:5962–5.